CATHODIC CAPACITY OF ALLOY 22 IN THE POTENTIAL YUCCA MOUNTAIN REPOSITORY ENVIRONMENT

P.K. Shukla,[1] R. Pabalan,[1] T. Ahn,[3] L. Yang,[2] X. He,[1] and H. Jung[1]

[1]Center for Nuclear Waste Regulatory Analyses
[2]Southwest Research Institute®
6220 Culebra Road
San Antonio, Texas 78238-5166
E-mail: pshukla@swri.org
Telephone: (210) 522-6534

[3]U.S. Nuclear Regulatory Commission
Two White Flint North
11545 Rockville Pike
Washington, DC 20555

ABSTRACT

The U.S. Department of Energy (DOE) has indicated that it may use Alloy 22 as the waste package outer container material for the potential high-level waste repository at Yucca Mountain, Nevada. Long-term corrosion performance of Alloy 22 is key to containment of radionuclides within the potential repository. Even though Alloy 22 exhibits high corrosion resistance in many environments, it could be susceptible to localized corrosion when exposed to either saturated solutions formed by dust deliquescence or seepage water brines at elevated temperatures. Localized corrosion in the form of crevice corrosion could persist if certain environmental and electrochemical conditions prevail in the repository drift environment. A one-dimensional physico-chemical analytical model has been developed to evaluate the effect of brine quantity and electrochemical conditions on the localized corrosion process. The model is then used to estimate the electrochemical conditions necessary for sustained propagation of localized corrosion at a given crevice site. The model is implemented for both saturated solutions arising from dust deliquescence and seepage water brines that may form inside the drifts of the potential Yucca Mountain repository. The simulation results indicate that for both brines, a sufficiently high positive difference between corrosion and repassivation potentials is needed for sustained propagation of crevice corrosion.

Keywords: localized corrosion, dust deliquescence brines, repassivation potential, seepage water brines, elevated temperatures, cathodic capacity, Alloy 22

INTRODUCTION

DOE has indicated that it may use Alloy 22 as the waste package outer container material for long-term disposal of high-level nuclear waste at the potential Yucca Mountain repository.[1] Long-term corrosion performance of Alloy 22 is key to containment of radionuclides within the potential repository. Under certain environmental and electrochemical conditions, Alloy 22 could undergo localized corrosion in the potential repository in-drift environment. Thermal-hydrological studies have shown that in-drift environmental conditions are a strong function of waste package temperature.[2,3] The waste package surface temperature is expected to initially increase after repository closure and decrease thereafter due to decay heat of the waste form.

In parallel, the relative humidity in the in-drift environment is expected to increase as the waste package surface temperature decreases. As a result, the initial dry environment in the repository drift will be followed by a wet environment where the waste package outer container material could degrade due to various corrosion processes, including general and localized corrosion.[4,5,6,7]

The evolution of the repository in-drift environment in terms of relative humidity is schematically represented in Figure 1. Alloy 22 could undergo aqueous corrosion in the form of general and localized corrosion when the relative humidity is greater than a threshold value (denoted by RH2 in Figure 1). The environment at relative humidities higher than RH2 can be divided into three categories: (i) ENV I, (ii) ENV II, and (iii) ENV III.

In ENV I, aqueous brines could develop by deliquescence of salts deposited with dusts on the waste package surface.[8] In ENV II, brines could form by evaporation of initially dilute seepage water that enters the repository drift. In ENV III, the water contacting the waste package essentially will be dilute seepage water. Both general and localized corrosion of Alloy 22 could occur in ENV I and II, whereas only general corrosion will likely occur in ENV III.[9,10,11,12]

In localized corrosion processes, metal corrodes at certain preferential sites at an accelerated rate. Localized corrosion of metals and alloys can occur in the form of pitting or crevice corrosion. Pitting corrosion of Alloy 22 is not expected in the potential repository environment.[13,14] However, localized corrosion in the form of crevice corrosion could initiate when the corrosion potential is greater than the crevice corrosion repassivation potential. The localized corrosion sites will remain active as long as the corrosion potential exceeds the repassivation potential[7,12,15] and there is sufficient cathodic current available to balance the anodic currents generated by metal dissolution reactions.[16,17] In the absence of either condition, localized corrosion could stifle and even repassivation may occur. The cathodic and anodic reaction sites are physically separated in the crevice corrosion process. Cathodic reactions dominate in the cathodic area, and the current generated in the cathodic area is referred as cathodic capacity. The oxygen reduction reaction is the dominant cathodic reaction within the expected range of conditions at the potential repository drift environment, and a sufficient cathodic capacity is needed for a sustained propagation of crevice corrosion at a sufficiently high rate.

The cathodic capacity is affected by the following factors: (i) oxygen reduction kinetics; (ii) environmental conditions such as temperature, pH, and chemical composition of brines; (iii) electrochemical conditions, such as corrosion potential, repassivation potential, and passive current density; and (iv) quantity of available electrolytes. The waste package surface is expected to be covered by only a thin brine film in both dust deliquescence[18] and seepage brine scenarios.[19] The thickness and length of the brine film is expected to play a major role in determining the cathodic capacity. At constant ionic conductivity and length of the brine film, the resistance to ionic flow and the corresponding ohmic potential drop increases as the thickness of the brine film decreases. For this reason, an evaluation of the effect of the characteristics of brine films on cathodic capacity is needed.

The objective of this work is to estimate the cathodic capacity of Alloy 22 in dust deliquescence and seepage brines and evaluate the role of two primary factors: (i) the electrochemical conditions and (ii) the quantity of the brine, which is represented by the thickness and length of a brine film uniformly spread near the crevice region. To this end, a one-dimensional

physico-chemical process model is developed to estimate the cathodic capacity. The interplay of oxygen reduction kinetic phenomenon with brine quantity is integrated into the model, which is used to calculate the electrode potential and current distribution in the cathodic region as a function film height, length, and electrochemical and environmental conditions for both dust deliquescence and seepage water brines. The current distribution in the cathodic region is then integrated to obtain the cathodic capacity for a given set of conditions. The information generated from cathodic capacity calculations is used to estimate the crevice penetration rate for a fixed area of the crevice site.

CATHODIC CAPACITY MODEL

For corrosion-resistant materials such as Alloy 22, it is widely accepted that localized corrosion in the form of crevice corrosion could initiate in the long term when the corrosion potential is greater than the repassivation potential. This statement can be represented by the following expression:

$$E_{corr} - E_{rp} > 0 \tag{1}$$

where

E_{corr} — corrosion potential [V]

E_{rp} — repassivation potential [V]

In crevice corrosion, the anodic and cathodic sites are physically separated. It is postulated that the crevice region will become deficient in oxidants due to the physical barrier to diffusional flow provided by the restricted geometry of the crevice former once the oxidant is consumed. As a result, the metal dissolution reaction dominates in the crevice region, whereas cathodic reactions dominate in the area adjacent to the crevice. A schematic of the crevice corrosion process is presented in Figure 2. As depicted in the figure, the anodic dissolution reactions predominantly occur in the crevice region formed underneath the crevice former. A generic form of the metal dissolution reaction can be represented by the following expression:

$$\mathrm{M} + y\mathrm{H_2O} \rightarrow \mathrm{M(OH)}_y + y\mathrm{H^+} + y\mathrm{e^-} \tag{2}$$

where metal M reacts with the water molecules to produce metal hydroxide, hydrogen ions, and free electrons.

In the potential Yucca Mountain repository environment, the dominant oxidant is expected to be oxygen. In the region outside the crevice, the oxygen reduction reaction will take place under mild oxidizing conditions in neutral-to-alkaline aerated solutions. This reaction can be expressed as

$$\mathrm{O_2} + 2\mathrm{H_2O} + 4\mathrm{e^-} \rightarrow 4\mathrm{OH^-} \tag{3}$$

In acidic solutions, the dissolved oxygen molecules are reduced according to the following expression:

$$\mathrm{O_2} + 4\mathrm{H^+} + 4\mathrm{e^-} \rightarrow 2\mathrm{H_2O} \tag{4}$$

It is assumed that in acidic solutions, the contribution of the hydrogen evolution reaction is negligible compared to that of oxygen reduction. This assumption is justifiable because the equilibrium potential of the hydrogen evolution reaction is expected to be much lower than that of the oxygen reduction reaction.[20] For the same reason, the contribution of the water reduction reaction to the cathodic current in neutral-to-alkaline solutions is expected to be negligible.

Under a steady-state crevice corrosion process, the sum of net current generated by the anodic and cathodic reactions must be equal to zero to maintain charge neutrality. This statement can be represented by the following equation:

$$I_A + I_C = 0 \tag{5}$$

where

I_A — net anodic current generated by metal dissolution reactions [A]

I_C — net cathodic current generated by the oxygen reduction reaction [A]

The cathodic capacity is equal to the net cathodic current, I_C. For a given set of electrochemical conditions that would initiate localized corrosion, the net cathodic current can be calculated with relative ease in both acidic and neutral-to-alkaline solutions because sufficient information exists on the kinetics of oxygen reduction reactions in both types of solutions.

Excess cathodic current is generated in the cathodic region because of a potential gradient in the electrolyte solution. The electrode potential is expected to be close to the repassivation potential at the crevice and cathodic region interface, and the electrode potential farther into the cathodic region must be equal to the corrosion potential. As a result, a gradient of electrolyte potential is established in the cathodic region. The current density generated at a given location in the cathodic region is determined by the polarization curve of the oxygen reduction reaction. A schematic of the cathodic region with appropriate boundary conditions and a corresponding oxygen reduction polarization curve is presented in Figure 3. As indicated in the polarization curve, the electrode potential is equal to the repassivation potential at the interface of the two regions. The oxygen reduction current density near the repassivation potential is markedly higher than at the corrosion potential. As the electrode potential approaches the corrosion potential, the oxygen reduction reaction current density decreases. Thus, the electrode potential distribution in the cathodic region and the corresponding potential dependence of oxygen reduction kinetics are the sources of excess cathodic current.

In the cathodic region, the current density due to the oxygen reduction reaction is determined by the interplay between the flow of current and the potential drop in the electrolyte, and the activation overpotential as a function of the distance from the crevice mouth. The passage of current in the electrolyte leads to the potential drop governed by Ohm's law, which can be expressed by the following equation:

$$i = -\kappa \frac{d\phi}{dx} \tag{6}$$

where

i — current density flowing through the electrolyte solution [A/cm^2]

κ — conductivity of the electrolyte solution [ohm^{-1}cm^{-1}]

ϕ — electrostatic potential of the electrolyte at a given location [V]

x — position vector [m]

The current flowing along the cathode surface varies with position due to the oxygen reduction reaction. This variation in current as a function of position can be expressed by the following equation:

$$\frac{di}{dx} = \frac{\left[j(x) + i_p \right]}{H} \tag{7}$$

where

$j(x)$ — current density [A/cm^2] generated by the cathodic reduction reaction current at position x

H — height of the electrolyte film [m]

i_p — passive current density [A/cm^2]

The combination of Eq. (6) and (7) yields

$$\frac{d^2\phi}{dx^2} = -\frac{\left[j(x) + i_p \right]}{\kappa H} \tag{8}$$

The current density generated due to the cathodic reduction reaction, $j(x)$, can be expressed by the following equation:

$$j(x) = -\frac{i_{corr} \exp\left[\frac{-\alpha_c nF}{RT} \left(V - \phi(x) - E_{corr} \right) \right]}{1 + \frac{i_{corr}}{i_{lim}} \exp\left[\frac{-\alpha_c nF}{RT} \left(V - \phi(x) - E_{corr} \right) \right]} \tag{9}$$

where

E_{corr} — corrosion potential [V]

i_{corr} — corrosion current density at the corrosion potential (equal to passive current density, i_p) [A/cm^2]

α_c — charge transfer coefficient for the cathodic reduction reaction

n — number of electrons per molecule of oxygen in the cathodic reduction reaction = 4

F — Faraday constant = 96,486 C/mol

R — universal gas constant = 8.3145 J/K/mol [1.987 cal/K/mol]

T — temperature of the system [K]

V — metal potential [V]

$\phi(x)$ — solution potential adjacent to the metal surface at position x

i_{lim} — mass-transfer-limited current density [A/cm^2]

The cathodic reaction can be either under activation or concentration control. If the cathodic reduction reaction is under concentration control, the current density will be equal to the mass-transfer-limited current density; otherwise, the reduction reaction current density under pure activation control is equal to the numerator of Eq. (9). For a given thickness of electrolyte film, the mass-transfer-limited current density can be calculated by the following equation:

$$i_{\lim} = \frac{nFDC_b}{H} \tag{10}$$

where

C_b — dissolved concentration of oxygen in the bulk electrolyte solution [mol/cm^3]

D — diffusivity of dissolved oxygen in the electrolyte solution [cm^2/sec]

The boundary conditions for Eq. (8) are the following. At the crevice and cathodic region interface, the electrode potential, which is equal to the potential drop across the metal-solution interface, is assumed to be the repassivation potential. This is a reasonable assumption given that very little or no cathodic current can be generated inside the crevice. This boundary condition can be represented by the following equation:

$$V - \phi(x = 0) = E_{rp} \tag{11}$$

Under free corrosion condition, the metal potential, denoted by V, is equal to zero. At the cathodic region and air interface, the following boundary condition prevails:

$$-\kappa \left.\frac{d\phi}{dx}\right|_{x=L} = 0 \tag{12}$$

Equation (12) represents the fact that no current can flow across the electrolyte and air interface.

Equation (8) is solved using MATLAB® Version 7.4.0 subjected to boundary conditions given by Eqs. (11) and (12). The solution of Eq. (8) is obtained in terms of the solution potential, ϕ, as a function of position vector, x. Then, the cathodic reduction current density, $j(x)$, is calculated for

each value of x using Eq. (9). The net cathodic current is calculated by numerically integrating the cathodic reduction plus passive current density for a given length of the cathodic region according to the following equation:

$$I_C = \int_{x=0}^{x=L} \left[i_p + j(x) \right] dx \tag{13}$$

The net cathodic current calculated using Eq. (13) is in units of A/cm. Cathodic capacities are calculated assuming the brine film and the crevice region have a width of 1 cm [0.39 in]. This assumption is based upon a physical representation of the crevice region and brine film surrounding the crevice region where both regions extend infinitely along the width. This is a bounding assumption because a crevice region will be limited by the cylindrical shape of the waste package. As a result, only a fraction of the brine film surrounding the crevice region will generate excess cathodic current. The parameter values used in Eqs. (8), (9), and (10) are described in the following section.

MODEL PARAMETERS

The cathodic capacity model is simulated for dust deliquescence and seepage brines. The model needs the values of corrosion potential (E_{corr}), passive current density (i_{pass}), corrosion current density (i_{corr}), electrolyte conductivity (κ), dissolved oxygen concentration (C_b), diffusivity of the oxygen (D), film thickness (H), length (L), and repassivation potential (E_{rp}). It is assumed that the available brine quantity is uniformly spread in the cathodic region located adjacent to the crevice (see Figure 3). The value of the cathodic reduction reaction charge transfer coefficient, denoted by α_c in Eq. (9), is set equal to 0.49, and the value of oxygen diffusivity is set equal to 10^{-5} cm^2/sec [1.55×10^{-6} in^2/sec]. These two values are adopted from reported experimental results on oxygen reduction kinetics on Alloy 22.[21] For both types of electrolyte solutions, values of corrosion potential, passive current density, electrolyte conductivity, and dissolved oxygen concentration are obtained from previously published works cited in the following two subsections. The values of film length and thickness and repassivation potential are varied and their effects on cathodic capacity are studied in this paper.

The parameter values for dust deliquescence and seepage brines are explained in the following subsections.

Dust Deliquescence Brine:

Deliquescence is a process in which a hygroscopic salt absorbs water vapor from humid air to form a saturated electrolyte solution. The formation of deliquescence brines is a concern for the potential Yucca Mountain repository because these brines could cause corrosion of the waste package at elevated temperatures. Some salts, particularly NaCl–$NaNO_3$–KNO_3 mixtures that could be important deliquescent mineral assemblages at Yucca Mountain,[22] have deliquescence points exceeding 180 °C [356 °F].[8] Table 1 lists the assemblage of various salts that could deliquesce at elevated temperature in ENV I.

The deliquescence brine properties needed to calculate the cathodic capacity of Alloy 22 are the brine film thickness and length, the effective ionic conductivity of the brine solution, and the dissolved oxygen concentration. Several assumptions are necessary to derive these properties.

The amount of dust on the metal surface is assumed to be 26 mg/cm^2 [0.37 mlb/in^2]. This amount is considered by DOE to be an upper bound value for dust that could deposit on the waste package surface in the potential Yucca Mountain repository.[18] The dust particles are assumed to have a specific density of 1 g/cm^3 [36.13 mlb/in^3] and a spherical diameter equal to either 10 or 30 μm [0.39 or 1.18 mils], based on the density and upper-bound estimates of particle size reported by DOE.[18] From the specific density of 1 g/cm^3 [36.13 mlb/in^3], the number of particles per square centimeter of metal surface corresponding to 26 mg [5.73×10^{-2} mlb] of dust is calculated to be 4.97×10^7 for 10 μm [0.39 mils] diameter particles or 1.84×10^6 for 30 μm [1.18 mils] diameter particles. Based on geometric considerations and assuming cubic packing of particles, this number of particles in one square centimeter is calculated to occupy 50 particle layers if the particle diameter is 10 μm [0.39 mils], or 17 particle layers if the particle diameter is 30 μm [1.18 mils]. Again, based on geometric considerations, the interparticle pore space is calculated to be 2.4×10^{-2} cm^3 [1.46×10^{-3} in^3] for the 50 particle layers and 2.38×10^{-2} cm^3 [1.45×10^{-3} in^3] for the 17 particle layers for 10 μm [0.39 mils] and 30 μm [1.18 mils] diameter particles, respectively, in 1 cm^2 [0.16 in^2] of the waste package surface. These results are summarized in Table 2.

To calculate the thickness of the brine film resulting from deliquescence, it is assumed that 10 weight percent of the dust that deposits on the metal surface comprises deliquescent salt {2.6 g/cm^2 [36.98 mlb/in^2]}. The 10 weight percent value is based on the average weight percent reported in the literature[23] for dust samples taken from the vicinity of Yucca Mountain. The deliquescent salt composition is assumed to be a NaCl–$NaNO_3$–KNO_3 mixture. At a temperature of 150 °C [302 °F], this salt mixture would deliquesce when the relative humidity in the environment reaches 17.7% and would form a saturated electrolyte solution with a density of 1.29 g/cm^3 [46.6 mlb/in^3]. The deliquescence relative humidity (or deliquescence point) and the brine density are calculated using StreamAnalyzer Version 2.0,[24] which is one of several software packages developed by OLI Systems, Inc., for evaluating the thermodynamic and transport properties of aqueous components in a chemical process for industrial and environmental applications. At the deliquescence point of the NaCl–$NaNO_3$–KNO_3 salt mixture, the electrolyte solution is calculated to have a composition of 69.6, 4.07, and 61.6 molal of KNO_3, NaCl, and $NaNO_3$, respectively. The amount of brine that forms is limited by the amount of deliquescent salt. Given that only 2.6 g/cm^2 [36.98 mlb/in^2] of salts are present on the metal surface, the calculated mass of water that forms upon deliquescence is 2.08×10^{-4} g/cm^2 [2.96×10^{-3} mlb/in^2]. The brine volume corresponding to this mass of water is 2.18×10^{-3} cm^3 [1.33×10^{-4} in^3], based on a brine density of 1.29 g/cm^3 [46.6 mlb/in^3]. The brine would occupy the interparticle pore spaces and would have a film thickness equivalent to 4.54 layers of 10-μm [0.39-mils]-diameter particles or 1.52 layers of 30-μm [1.18-mils]-diameter particles. A schematic representation of spreading of the brine film layer with dust particles is represented in Figure 4 which shows that the thickness of brine film is less than that of the dust layer.

The ionic conductivity of the deliquescence brine at 150 °C [302 °F] calculated from StreamAnalyzer Version 2.0 is 0.0382 ohm^{-1}cm^{-1} [0.0971 ohm^{-1}in^{-1}]. However, the effective ionic conductivity of the electrolyte is decreased by the presence of the dust particles. The effective ionic conductivity can be calculated using Bruggeman's equation:[25]

$$k_{eff} = k(\Theta)^{1.5} \tag{14}$$

where

$$\Theta = \frac{V_{solution}}{V_{solution} + V_{particle}} \quad (15)$$

and

$V_{solution}$ — volume occupied by the solution [cm^3]

$V_{particle}$ — volume occupied by the particles [cm^3]

k — ionic conductivity of the pure electrolyte solution [$ohm^{-1}cm^{-1}$]

k_{eff} — effective ionic conductivity of the electrolyte solution in the presence of particles [$ohm^{-1}cm^{-1}$]

For the brine with a film thickness equivalent to 4.54 particle layers, the value of Θ is calculated to be 0.480 and the effective ionic conductivity is equal to 0.01834 $ohm^{-1}cm^{-1}$ [0.04658 $ohm^{-1}in^{-1}$]. For the brine with a film thickness of 1.52 particle layers, Θ is calculated to be 0.478 and the effective ionic conductivity is equal to 0.01826 $ohm^{-1}cm^{-1}$ [0.04638 $ohm^{-1}in^{-1}$]. Because the relative difference between the two calculated values for both particle sizes is less than 1 percent, the effective ionic conductivity of 0.01834 $ohm^{-1}cm^{-1}$ [0.04658 $ohm^{-1}in^{-1}$] is used in cathodic capacity simulations for dust deliquescence brines. The ionic conductivity and effective ionic conductivity of dust deliquescence brines for both particle sizes are also summarized in Table 2.

The dissolved oxygen concentration in the deliquescence brines at various temperature is calculated using the model presented in Tromans[26,27] and the StreamAnalyzer-calculated brine composition, which is mentioned in a preceding paragraph. Tromans[26,27] gives equations for calculating the effect of electrolytes, including NaCl and $NaNO_3$, on the dissolved oxygen concentration. However, no parameters were provided for KNO_3 solutions. Therefore, for this study, it is assumed KNO_3 has the same effect on oxygen solubility as $NaNO_3$, and the dissolved oxygen concentration in NaCl-$NaNO_3$-KNO_3 solutions is calculated using NaCl and $NaNO_3$ parameters only. The dissolved oxygen concentration for various salt assemblages is summarized in Table 1. It can be noticed that the dissolved oxygen concentration does not change much for different salt assemblages at various temperatures. For this reason, the dust deliquescence brine temperature is selected to be 150 °C [302 °F] for calculating cathodic capacity of Alloy 22 in these brines.

The corrosion potential of Alloy 22 in dust deliquescence brines is selected to be 0.6 V_{SHE}, where SHE stands for standard hydrogen reference electrode. This value is based on the experimental studies conducted by Yang[28] in which the corrosion potential of Alloy 22 in dust deliquescence brine was recorded in the range of 0.4 to 0.65 V_{SHE}.

At the corrosion potential, the corrosion and passive current density are calculated using the following equation:

$$i_{corr} = i_{pass} = i_a^0 \exp\left[-\frac{E}{R}\left(\frac{1}{T} - \frac{1}{T_{ref}}\right)\right] \quad (16)$$

where

T — temperature of the system [K]

i_a^0 — passive current density (A/cm^2) at temperature T_{ref}[K] = 10^{-8}A/cm^2 [6.45 × 10^{-8}A/in^2]

E — activation energy [J/mol] for the passive current density = 44,700 J/mol [10,676 cal/mol]

R — universal gas constant = 8.3145 J/K /mol [1.987 cal/K/mol]

T_{ref} — reference temperature [K] for the passive current density = 368.15 K [203 °F]

Eq. (16) is used to calculate the passive current at 150 °C [302 °F] for dust deliquescence brines. Dunn, et al.[12] originally proposed this equation, derived from their own experimental data, for calculating the passive current density and the corresponding general corrosion rate in seepage water brines. It is noted that the corrosion rate estimated using Eq. (16) is also within the range of corrosion rates in dust deliquescence brines experimentally observed by Yang.[28]

Seepage Brine:

Seepage water entering the emplacement drifts of a potential repository initially will be dilute with the chemical composition of pore waters. However, evaporative processes will cause brines to form that could initiate crevice corrosion of the Alloy 22.[13] The initiation of localized corrosion in ENV II is determined by the repassivation potential and the corrosion potential.

The corrosion potential of the waste package material is a function of brine water chemistry, temperature, and oxidation–reduction kinetics. Dunn, et al.[12] developed a corrosion potential model for Alloy 22 for seepage brines in the Yucca Mountain repository environment based upon electrochemical kinetic laws and adjusted the model to experimentally measured values. This model is represented by the following equation:

$$E_{corr} = \frac{E_a^a - E_a^{ef}}{Z_r \beta_r^{ef} F} - \frac{E_a^a T}{Z_r \beta_r^{ef} F T_{ref}^a} + \frac{RT}{Z_r \beta_r^{ef} F} ln\left[\left(\frac{[H^+]}{1\ mol/L}\right)^{n_o}\left(\frac{pO_2}{1\ atm}\right)^{n_H} \frac{i_r^{ref}}{i_a^o} \frac{C_{O_2}^{bulk}(T)}{C_{O_2}^{bulk}(T_{ref})}\right] \quad (17)$$

where

E_{corr} — corrosion potential (Volts vs. Standard Hydrogen Electrode)

E_a^a — activation energy for the anodic current density [J/mol]

E_a^{ef} — effective activation energy [J/mol]

Z_r — number of electrons in the oxygen reduction reaction, 4

T_{ref} — reference temperature [K] = 298.15 K [77 °F]

i_a^o — anodic current density at reference temperature (A/cm^2)

i_r^{ref} — reference current density (A/cm^2)

F — Faraday constant = 96,486 C/mol

$C_{O_2}^{bulk}(T)$ — dissolved oxygen concentration in solution as a function of temperature [mol/kg]

$C_{O_2}^{bulk}(T_{ref})$ — dissolved oxygen concentration in solution at the reference temperature [mol/kg]

β_r^{ef} — dimensionless effective charge transfer coefficient

T_{ref}^{a} — reference temperature for anodic current density [K]

T — temperature of the system [K]

n_H, n_o — dimensionless constant

pO_2 — partial pressure of oxygen in atmosphere, 0.21 atmosphere [3.09 psi]

$[H^+]$ — hydrogen ion concentration [M], 10^{-pH}

The corrosion potential model of Dunn, et al.[12] uses the following equation from Battino[29] to calculate the dissolved oxygen concentration as a function of temperature:

$$C_{O_2}^{bulk}(T) = pO_2 e^{0.2984 - \frac{5.5961\times10^3\ K}{T} + \frac{1.04967\times10^6\ K^2}{T^2}}\ mol\ kg^{-1}\ atm^{-1} \qquad (18)$$

where

$C_{O_2}^{bulk}(T)$ — dissolved oxygen concentration in aqueous solution at temperature T

T — temperature (K)

pO_2 — partial pressure of oxygen in atmosphere, 0.21 atmosphere [3.09 psi]

Table 3 lists the parameter values used in Eq. (17). The calculated corrosion potential as a function of pH at various temperatures is presented in Figure 5. The corrosion potential model was developed using electrochemical kinetic laws. Model parameters in Eq. (17) were selected to account for experimentally measured general corrosion rates at low and high pH.[12,30] As a first approximation in the model, a sharp transition in the corrosion potential was selected at pH equal to 6. The transition is attributed to different regimes of the oxygen reduction reactions. The reduction reaction represented by Eq. (3) is expected to dominate in neutral-to-alkaline solutions and by Eq. (4) in acidic solutions. For cathodic capacity calculations, the pH and temperature of the brine are specified and the corrosion potential is calculated. The passive and corrosion current densities at a given temperature are then calculated using Eq. (16).

As stated previously, the corrosion potential of Alloy 22 is a function of brine water chemistry. The chemistry of the brine that results from evaporation of seepage waters will depend on the composition of the initially dilute waters. Previous studies have used thermodynamic simulations to determine the range in composition of seepage brines that could form at the potential Yucca Mountain repository.[31,32,33] For example, Pensado and Pabalan[33] used StreamAnalyzer Version 2.0 to calculate the range in brine chemistry that could form if evaporation occurs at a temperature of 110 °C [230 °F]. The results were reported for three water types: alkaline, neutral, and calcium-chloride brines. The values of ionic conductivity and chloride ion concentration of these three waters calculated using StreamAnalyzer Version 2.0

are plotted in Figures 6(a) and 6(b), respectively. To calculate the cathodic capacity of Alloy 22 in saturated seepage brines, values of pH and ionic conductivity are needed as input to the model. For this study, a pH value of 10.9 and ionic conductivity of 0.778 $ohm^{-1}cm^{-1}$ [1.976 $ohm^{-1}in^{-1}$] are used. These values correspond to the median values of pH and ionic conductivity calculated by Pensado and Pabalan[33] for alkaline-type waters, which is the expected dominant water type at Yucca Mountain. The temperature of the seepage brine is assumed to be 110 °C [230 °F] for calculating cathodic capacity of Alloy 22.

RESULTS

The cathodic capacity model is implemented for dust deliquescence and seepage brines using parameter values described in the previous section. The simulation results are described in the following subsections.

Dust Deliquescence:

The distribution of potential drop across the metal–solution interface (i.e., electrode potential) as a function of distance from the crevice region is presented in Figure 7(a). Four electrode potential distributions are presented corresponding to four film thicknesses: 1, 25, 45, and 100 μm [3.94×10^{-2}, 0.98, 1.8, 3.94 mils]. These four simulations are performed using a repassivation potential equal to 0.1 V_{SHE}. As seen in Figure 7(a), the electrode potential increases more sharply for a 1-μm [3.94×10^{-2}-mils]-thick film compared to the thicker films and attains a value equal to the corrosion potential at a distance approximately 0.06 m [2.36 in] from the crevice region. This result is consistent with the formulation of solution potential distribution represented by Eq. (8). An analysis of Eq. (8) indicates that solution potential is inversely proportional to the product of electrolyte ionic conductivity and film thickness. Therefore, the solution potential along the metal surface would decrease sharply for thin films. The corresponding current density distributions for four film thicknesses are presented in Figure 7(b). The area under the current density distribution curves is equal to the cathodic capacity of the film. As seen in Figure 7(b), the area under the 1-μm [3.94×10^{-2}-mils]-thick film is smaller compared to the 25-μm [0.98-mils]-thick film. The area under the current density distribution curve increases with increasing thickness, which indicates the cathodic capacity also increases with film thickness for a given film length.

The cathodic capacities for various values of repassivation potential and film thickness are presented in Figure 8 where each data point represents cathodic capacity for one electrode potential and corresponding current density distribution. The corrosion potential and brine film length are set equal to 0.6 V_{SHE} and 0.1 m [3.94 in], respectively. The cathodic capacity is presented as a function of the difference between corrosion potential and repassivation potential, (i.e., $E_{corr}–E_{rp}$). As seen in the figure, the cathodic capacity increases with increasing values of $E_{corr}–E_{rp}$. On other hand, the cathodic capacity increases with film thickness for a fixed value of $E_{corr}–E_{rp}$. However, for 1-μm [3.94×10^{-2}-mils]-thick film, the electrode potential distribution presented in Figure 7(a) indicate that cathodic capacity reaches an anymptotic value at a fixed value of $E_{corr}–E_{rp}$ (i.e., additional increases in film length will not result in further increases in cathodic capacity). This behavior is due to the fact that the electrode potential attains an asymptotic value of corrosion potential close to the crevice region even for large values of $E_{corr}–E_{rp}$. However, for thicker films and for a given value of $E_{corr}–E_{rp}$, a marginal increase in cathodic capacity may result because of an increase in film length.

To explore the effect of brine film length on cathodic capacity, additional simulations are performed at a fixed film thickness but variable film length. The simulation results are presented in Figure 9, where cathodic capacity is plotted as a function of $E_{corr}–E_{rp}$. The brine film thickness and corrosion potential are set equal to 45 μm [1.8 mils] and 0.6 V_{SHE}, respectively. As seen in the figure, there is a marginal variation in cathodic capacity with increasing film length. This result is consistent with the observation that the electrode potential changes sharply near the crevice region. As a result, most of the excess cathodic current density is generated in the cathodic region adjacent to the crevice. For this reason, an increase in film length has only a marginal effect on cathodic capacity of Alloy 22 in dust deliquescence brines. In Figures 8 and 9, a horizontal dash line is added to emphasize the consequence of cathodic capacity values above the dash line. Cathodic capacity greater than 9.8×10^{-6} A/cm [2.49×10^{-5} A/in] at a given $E_{corr}–E_{rp}$ will result in penetration rate of 100 μm/year [3.94 mils/year] or higher for an active crevice area of 1 cm^2 [0.16 in^2].

Seepage Brines:

Cathodic capacity of Alloy 22 in seepage water brines as a function of $E_{corr}–E_{rp}$ is plotted in Figure 10. The results shown in the figure are calculated for various brine film thicknesses but a fixed film length of 0.1 m [3.94 in]. The brine temperature and pH are set equal to 110 °C [203 °F] and 10.9, respectively. The corrosion potential is calculated using Eq. (17), and the repassivation potential is varied. The calculated results show that at $E_{corr}–E_{rp}$ less than 0.3 V, the cathodic capacity changes only slightly with different brine film thicknesses. However, at $E_{corr}–E_{rp}$ greater than 0.3 V, a large variation in cathodic capacity with brine film thickness is observed. This behavior occurs due to a change in mass-transfer-limited current with film thickness. When $E_{corr}–E_{rp}$ is greater than 0.3 V, a substantial part of the cathodic region is under concentration polarization. As a result, the cathodic current density is equal to the mass-transfer-limited current [see Eq. (10)], which decreases with increasing film thickness. Therefore, the cathodic capacity also decreases with increasing film thickness. However, when $E_{corr}–E_{rp}$ is less than 0.3 V, most of the cathodic region is under activation control, and cathodic current density is minimally affected by the mass-transfer-limited current.

The cathodic capacity as a function of $E_{corr}–E_{rp}$ for different brine film lengths is presented in Figure 11. As seen in the figure, the cathodic capacity of Alloy 22 at a given value of $E_{corr}–E_{rp}$ varies significantly with film length. This result is in contrast to the calculated cathodic capacity of Alloy 22 in the presence of dust deliquescence brines where film length has only a marginal effect. This difference can be attributed to the higher ionic conductivity of seepage brines compared to that of dust deliquescence brines. Because of this factor, the change in solution potential along the film length in seepage brines is less pronounced compared to the dust deliquescence brine. As a result, excess cathodic current is generated even in the cathodic region farther away from the crevice region. In Figures 10 and 11, a horizontal dashed line is drawn to emphasize the consequence of higher cathodic capacity. When the cathodic capacity exceeds 9.8×10^{-6} A/cm [2.49×10^{-5} A/in] at a given $E_{corr}–E_{rp}$, a penetration rate of 100 μm/year [3.94 mils/year] or higher would be observed for an active crevice area of 1 cm^2 [0.16 in^2]. For seepage water brine, the transition point shifts from 0.28 V for a 0.1-m [3.94-in]-long film to 0.18 V for a 0.5-m [1.64-ft]-long film. In summary, film length has a greater influence on cathodic capacity for seepage water brines compared to dust deliquescence brines.

DISCUSSION AND SUMMARY

The cathodic capacity of Alloy 22 in dust deliquescence brines formed in ENV I is determined primarily by the film thickness and by the difference between corrosion and repassivation potentials (i.e., $E_{corr}-E_{rp}$). This observation is deduced from the results presented in Figure 7. As seen in Figure 7(a), the potential at the metal–solution interface approaches the corrosion potential with increasing distance from the crevice, and the gradient of the potential is fairly steep at the interface. As a result, most of the excess cathodic current is generated where the electrode potential is sufficiently cathodic with respect to the corrosion potential. Even though excess cathodic current also is generated farther into the cathodic region, the magnitude of the excess current is too small to have a significant influence on the cathodic capacity. Therefore, a sufficiently long brine film {0.1 m [3.94 in]} is needed adjacent to the crevice mouth for generating the excess cathodic current, and a film extending farther than 0.1 m [3.94 in] into the cathodic region does not have much influence on the cathodic capacity. This observation is confirmed by the results presented in Figure 9, where cathodic capacity is plotted as a function of $E_{corr}-E_{rp}$ for various film lengths at a film thickness equal to 45 μm [1.8 mils]. The calculated cathodic capacity does change only marginally with increasing film length for a given value of $E_{corr}-E_{rp}$. Therefore, it is concluded that cathodic capacity of Alloy 22 in dust deliquescence brines is primarily dependent on $E_{corr}-E_{rp}$ and film thickness as long as the film length is 0.1 m [3.94 in] or more.

The cathodic capacity of Alloy 22 in saturated seepage water brines formed during ENV II is dependent on film thickness, film length, and $E_{corr}-E_{rp}$. Because brine quantity is not limited for seepage waters, the brine film thickness will be governed by the competition between gravitational and surface tension forces on the Alloy 22 surface. An analysis to determine the seepage water brine film thickness is outside the scope of this paper. For this reason, cathodic capacity is calculated at several values of brine film thicknesses. The results presented in Figure 10 indicate that cathodic capacity does not change significantly with film thickness as long as $E_{corr}-E_{rp}$ is less than 0.3 V. However, cathodic capacity varies significantly with film thickness when $E_{corr}-E_{rp}$ is greater than 0.3 V. This observation is attributed to the interplay between mass-transfer-limited current and solution potential distribution in the thin film along the metal surface. When $E_{corr}-E_{rp}$ is higher than 0.3 V, a significant portion of the cathodic region lies under electrochemical conditions corresponding to concentration polarization control. The excess current in the concentration polarization region is derived from the mass-transfer-limited current, which varies inversely with film thickness. For this reason, cathodic capacity decreases with increasing film thickness when $E_{corr}-E_{rp}$ is greater than 0.3 V.

The effect of film length on the cathodic capacity of Alloy 22 in seepage water brines is demonstrated in Figure 11, where the cathodic capacity increases with increasing film length for a given value of $E_{corr}-E_{rp}$. This observation is attributed to the fact that the ionic conductivity of seepage brines is approximately 40 times higher than that of dust deliquescence brines. As a result, the solution potential varies less steeply along the metal surface and more effective cathodic area is available for the generation of excess cathodic current. For this reason, cathodic capacity increases with increasing film length in seepage water brines.

The effect of cathodic capacity on the crevice corrosion process can be understood by calculating the penetration rate for a given crevice site. A cathodic capacity of 9.8×10^{-6} A/cm [2.49×10^{-5} A/in] can sustain metal dissolution at the rate of 100 μm/yr [3.94 mils/yr] for 1 cm^2 [0.16 in^2] of active crevice area. A cathodic capacity of 9.8×10^{-6} A/cm [2.49×10^{-5} A/in] in dust

deliquescence brines is attained when $E_{corr} - E_{rp}$ is approximately equal to 0.4 V for a 45-μm [1.8-mils]-thick film (see Figure 8). The same cathodic capacity for seepage water brines is achieved when $E_{corr} - E_{rp}$ is approximately equal to 0.28 V for the 0.1-m [3.94-in]-long film (see Figure 10). The $E_{corr} - E_{rp}$ value decreases as film length is increased for the same cathodic capacity. As seen in Figure 11, the cathodic capacity of 9.8×10^{-6} A/cm [2.49×10^{-5} A/in] is achieved when $E_{corr} - E_{rp}$ is equal to 0.18 V for a 0.5-m [1.64-ft]-long film. However, the probability of having a long continuous film in ENV II is expected to be low because of the physical design of the waste package and the seepage mechanism of the in-drift water. It is expected that any seepage water will enter the repository drift through the dripping process from the drift crown.[13] Upon hitting the waste package, the water will splatter and drain away from the waste package surface. For this reason, the probability of having a long continuous film is expected to be lower than having a shorter film.

An analysis similar to one presented in the preceding paragraph can be carried out for evaluating the effect of cathodic capacity when the active crevice area is 0.1 cm^2 [0.16 in^2] or less. In such a case, a lower value of cathodic capacity may be sufficient to sustain a high penetration rate. For example, a cathodic capacity of 9.8×10^{-7} A/cm [2.49×10^{-6} A/in] in dust deliquescence brines at $E_{corr} - E_{rp}$ equal to 0.12 V for 45-μm [1.8-mils]-thick film can sustain a penetration rate of 100 μm/yr [3.94 mils/yr] in a 0.1 cm^2 [0.016 in^2] crevice area. However, a smaller crevice site will have less significance on the release of radionuclides compared to a larger site.

In summary, the results of the cathodic capacity model for dust deliquescence brines indicate that localized corrosion with a penetration rate of 100 μm/year [3.94 mils/year] for 1 cm^2 [0.16 in^2] of crevice can be achieved when $E_{corr} - E_{rp}$ is greater than 0.34 V for a 100-μm [3.94-mils]-thick film. The critical value of $E_{corr} - E_{rp}$ {i.e., when penetration rate is greater than 100 μm/year [3.94mils/year]} increases with decreasing film thickness. Similarly, the same penetration can be achieved with $E_{corr} - E_{rp}$ equal to 0.18 V for a 500-μm [19.7-mils]-thick and 0.5-m [1.64-ft]-long film of the seepage water brines, and the critical value of $E_{corr} - E_{rp}$ increases with increasing film length. However, no effect is observed on the critical value of $E_{corr} - E_{rp}$ with a change in film thickness at a fixed film length.

ACKNOWLEDGMENTS

The authors gratefully acknowledge the reviews of Drs. G. Cragnolino and D. Turner, the editorial review of L. Mulverhill, and the assistance of B. Street in the preparation of this manuscript.

This paper describes work performed by the Center for Nuclear Waste Regulatory Analyses (CNWRA) for the U.S. Nuclear Regulatory Commission (NRC) under contract number NRC–02–02–012. The activities reported here were performed on behalf of the NRC Office of Nuclear Material Safety and Safeguards, Division of High-Level Waste Repository Safety. This paper is an independent product of CNWRA and does not necessarily reflect the view or regulatory position of NRC. The NRC staff views expressed herein are preliminary and do not constitute a final judgment or determination of the matters addressed or of the acceptability of a license application for a potential geologic repository at Yucca Mountain.

REFERENCES

1. DOE. DOE/RW–539, "Yucca Mountain Science and Engineering Report," Las Vegas, Nevada: Office of Civilian Radioactive Waste Management, 2001.

2. R. Fedor, S. Green, D. Walter, G. Adams, D. Farrell, and S. Svedeman, "Temperature and Relative Humidity Along Heated Drifts With and Without Drift Degradation," CNWRA 2004-04, San Antonio, Texas: Center for Nuclear Waste Regulatory Analyses, 2004.

3. C. Manepally and R. Fedors, "Edge-Cooling Effect on the Potential Thermohydrologic Conditions at Yucca Mountain," Proceedings of the 10th International High-Level Radioactive Waste Management Conference, Las Vegas, Nevada, March 30–April 3, 2003, Published on CD-ROM, La Grange Park, Illinois: American Nuclear Society, 2003.

4. G.M. Gordon, "Corrosion considerations related to permanent disposal of high-level radioactive waste," Corrosion, Vol. 58, pp. 811–825, 2002.

5. Bechtel SAIC Company, LLC, "Technical Basis Document No. 6: Waste Package and Drip Shield Corrosion," Rev. 1, Las Vegas, Nevada: Bechtel SAIC Company, LLC, 2004.

6. Bechtel SAIC Company, LLC, "General Corrosion and Localized Corrosion of Waste Package Outer Barrier," Rev. 02, Las Vegas, Nevada: Bechtel SAIC Company, LLC, 2004.

7. D.S. Dunn, L. Yang, Y-M. Pan, and G.A. Cragnolino, "Localized Corrosion Susceptibility of Alloy 22," Proceedings of the CORROSION 2003 Conference, Paper No. 03697, Houston, Texas: NACE International, 2003.

8. J.A. Rard, K.J. Staggs, S.D. Day, and S.A. Carroll, "Boiling temperature and reversed eeliquescence relative humidity measurements for mineral assemblages in the NaCl + $NaNO_3$ + KNO_3 + $Ca(NO_3)_2$ + H_2O system," Journal of Solution Chemistry, Vol. 35, pp. 1187–1215, 2006.

9. L. Yang, "Corrosion of Alloy 22 in Concentrated Nitrate and Chloride Salt Environments at Elevated Temperatures—Progressive Report," CNWRA 2006-02, San Antonio, Texas: Center for Nuclear Waste Regulatory Analyses, 2006.

10. R.B. Rebak, "Newer Alloy 22 Data and Their Relevance to High-Temperature Localized Corrosion," Presentation at the NWTRB Workshop on Localized Corrosion of Alloy 22 in Yucca Mountain Environments, Las Vegas, Nevada, September 26, 2006.

11. S. Dixit, S. Roberts, K. Evans, T. Wolery, and S. Caroll, "General Corrosion and Passive Film Stability," UCRL-TR-217393, Livermore, California: Lawrence Livermore National Laboratory, 2006.

12. D.S. Dunn, O. Pensado, Y.-M. Pan, R.T. Pabalan, L. Yang, X. He and K.T. Chiang, "Passive and Localized Corrosion of Alloy 22-Modeling and Experiments," CNWRA 2005-02, Rev. 1, San Antonio, Texas: Center for Nuclear Waste Regulatory Analyses, 2005.

13. G.A. Cragnolino, D.S. Dunn, C.S. Brossia, V. Jain, and K.S. Chan, "Assessment of Performance Issues Related to Alternate Engineered Barrier System Materials and Design Options," CNWRA 99-003, San Antonio, Texas: Center for Nuclear Waste Regulatory Analyses, 1999.

14. G. E. Gdowski, "Survey of Degradation Models of Four Nickel-Chromium-Molybdenum Alloys," UCRL–1D–108330, Livermore, California: Lawrence Livermore National Laboratory, 1991.

15. F. Hua, J. Sarver, J. Jevec, and G. Gordon, "Corrosion behavior of Alloy 22 and Ti Grade 7 in a nuclear waste repository environment," Corrosion, Vol. 60, No 8, pp. 764–777, 2004.

16. F. Cui, F. Presuel-Moreno, and R. Kelly, "Computational modeling of cathodic limitation on localized corrosion of wetted SS 316 at room temperature," Corrosion Science, Vol. 47, pp. 2987–3005, 2005.

17. R.G. Kelly, A. Agarwal, F. Cui, X. Shan, U. Landau, and J. Payer, "Considerations of the Role of the Cathodic Regions in Localized Corrosion," 11th International High-Level Radioactive Waste Management Conference, Las Vegas, Nevada, April 30–May 4, 2006.

18. Bechtel SAIC Company, LLC, "Analysis of Dust Deliquescence for FEP Screening," ANL–EBS–MD–000074, Rev. 0, Las Vegas, Nevada: Bechtel SAIC Company, LLC, 2005.

19. Bechtel SAIC Company, LLC, "General Corrosion and Localized Corrosion of Waste Package Outer Barrier," Rev. 02, Las Vegas, Nevada: Bechtel SAIC Company, LLC, 2004.

20. A.J. Bard and L.R. Faulkner, "Electrochemical Methods, Fundamentals and Applications," New York City, New York: John Wiley & Sons, 1980.

21. A. Davydov, K. Rybalka, L. Beketaeva, G. Engelhardt, P. Jayaweera, and D. MacDonald, "The kinetics of hydrogen evolution and oxygen reduction on Alloy 22," Corrosion Science, Vol. 47, pp. 195–215, 2005.

22. C.R. Bryan, "Localized Corrosion Due to Dust Deliquescence on the Alloy 22 Waste Package Outer Barrier," Nuclear Waste Technical Review Board Meeting, November 8–9, 2005, Las Vegas, Nevada, 2005, <http://www.nwtrb.gov/meetings/nov%202005/bryan.pdf>

23. M.C. Reheis, "Dust Deposition in Nevada, California, and Utah, 1984-2002," U.S. Geological Survey, Open-File Report 03-138, 2003.

24. OLI Systems, Inc., “A Guide to Using the OLI Software for Version 2.0 of the Analyzers,” Morris Plains, New Jersey: OLI Systems, Inc., 2005.

25. D.A.G. Bruggeman, “Berechnung verschiedener physikalischer Konstanten von heterogenen Substanzen. I. Dielectrizitatskonstanten und Leitfahigkeiten der Mischkorper aus isotropen Substanzen,” Ann. Phys. Leipzig, Vol. 24, pp. 636–679, 1935.

26. D. Tromans, “Temperature and pressure dependent solubility of oxygen in water: a thermodynamic analysis,” Hydrometallurgy, Vol. 48, pp. 327–342, 1998.

27. D. Tromans, “Modeling oxygen solubility in water and electrolyte solutions,” Industrial & Engineering Chemistry Research, Vol. 39, pp. 805–812, 2000.

28. L. Yang, “Corrosion of Alloy 22 in Concentrated Nitrate and Chloride Salt Environments at Elevated Temperatures—Progress Report,” CNWRA 2006-02, San Antonio, Texas: Center for Nuclear Waste Regulatory Analyses, 2006.

29. R. Battino, ed., “International Union of Pure and Applied Chemistry (IUPAC) Solubility Data Series: Oxygen and Ozone,” New York City, New York: Pergamon Press, 1981.

30. O. Pensado, R. Pabalan, D. Dunn, and K.T. Chiang, “Use of Alloy-22 as a Long-Term Radioactive Waste Containment Material,” 9th International Symposium on the Passivation of Metals and Semiconductors and the Properties of Thin Oxides (Passivity-9),” Paris, France, June 27–July 1, 2005.

31. Bechtel SAIC Company, LLC, “Technical Basis Document No. 5: In-drift Chemical Environment, Rev. 1,” Las Vegas, Nevada: Bechtel SAIC Company, LLC, 2003.

32. R.T. Pabalan, L. Yang, and L. Browning, “Deliquescence behavior of multicomponent salts: effects on the drip shield and waste package chemical environment of the proposed nuclear waste repository at Yucca Mountain, Nevada,” P. McGrail, and G.A. Cragnolino, eds., Scientific Basis for Nuclear Waste Management XXV, Materials Research Society Symposium Proceedings, Vol. 713, Warrendale, Pennsylvania: Materials Research Society, pp. 37–44, 2002.

33. O. Pensado and R. Pabalan, “Understanding Conditions for Localized Corrosion and Stress Corrosion Cracking of Alloy 22 in Repository Settings,” 3rd International Workshop on Long-Term Prediction of Corrosion Damage in Nuclear Waste Systems, May 14–18, 2007, State College, Pennsylvania, 2007.

TABLE 1

DELIQUESCENCE RELATIVE HUMIDITY, DISSOLVED OXYGEN CONCENTRATION , AND IONIC CONDUCTIVITY OF DELIQUESCENCE SALTS AT VARIOUS TEMPERATURES

Temperature (°C) [°F]	Salts Present	Deliquescence Relative Humidity (percent)	Dissolved Oxygen Concentration (parts per million)	Ionic Conductivity ($ohm^{-1}cm^{-1}$) [$ohm^{-1}in^{-1}$]
120 [248]	$NaCl+NaNO_3+KNO_3$	26.7	0.334	0.035 [0.089]
130 [266]	$NaCl+NaNO_3+KNO_3$	22.2	0.347	0.033 [0.084]
140 [284]	$NaCl+NaNO_3+NaNO_3{\cdot}KNO_3$	18.2	0.365	0.032 [0.081]
150 [302]	$NaCl+NaNO_3+NaNO_3{\cdot}KNO_3$	17.7	0.386	0.038 [0.097]
160 [320]	$NaCl+NaNO_3+NaNO_3{\cdot}KNO_3$	16.5	0.412	0.042 [0.107]
170 [338]	$NaCl+NaNO_3+NaNO_3{\cdot}KNO_3$	14.6	0.443	0.042 [0.107]

TABLE 2

DUST PARTICLE SIZE, DUST LAYER AND BRINE FILM THICKNESS, AND IONIC CONDUCTIVITY AND EFFECTIVE IONIC CONDUCTIVITY OF DUST DELIQUESCENCE BRINE FORMED BY $NaCl+NaNo_3+NaNO_3•KNO_3$ SALT ASSEMBELAGE AT 150 °C [302 °F]

Particle Size (μm) [mils]	Dust Layer Thickness (μm) [mils]	Brine Film Thickness (μm) [mils]	Ionic Conductivity of $NaCl–KNO_3–NaNO_3$ Brine ($ohm^{-1}cm^{-1}$) [ohm^{-1} in^{-1}]	Effective* Ionic Conductivity of $NaCl–KNO_3–NaNO_3$ Brine ($ohm^{-1}cm^{-1}$) [ohm^{-1} in^{-1}]
10 [0.39]	500 [19.7] (50 particle layers)	45.4 [1.79]	0.0382 [0.0970]	0.01834 [0.04658]
30 [1.18]	510 [20.1] (17 particle layers)	45.6 [1.80]	0.0382 [0.0970]	0.01826 [0.04638]

Temperature = 150 °C [302 °F]; Deliquescence Relative Humidity = 17.7%
Brine composition: 69.6 molal KNO_3, 4.1 molal NaCl, 61.6 molal $NaNO_3$
*Calculated using Bruggeman's equation (Eq. 14)

TABLE 3

VALUES OF PARAMETERS USED IN EQ. (17) TO CALCULATE CORROSION POTENTIAL[12]

Parameter	Value at pH < 6	Value at pH > 6
E_a^a (J/mol) [cal/mol]	44,700 [10,676]	44,700 [10,676]
E_a^{ef} (J/mol) [cal/mol]	40,000 [9,553]	40,000 [9,553]
i_a^o (A/cm^2) [A/in^2]	10^{-8} [6.45×10^{-8}]	10^{-8} [6.45×10^{-8}]
T_{ref}^a (K) [°F]	368.15 [203]	368.15 [203]
T_{ref} (K) [°F]	298.15 [77]	298.15 [77]
β_r^{ef}	0.01287	0.0248
n_H	0.0256	0.01897
i_r^{ref} (A/cm^2) [A/in^2]	0.241 [1.55]	0.175 [1.13]
n_o	0.01287	0.0248

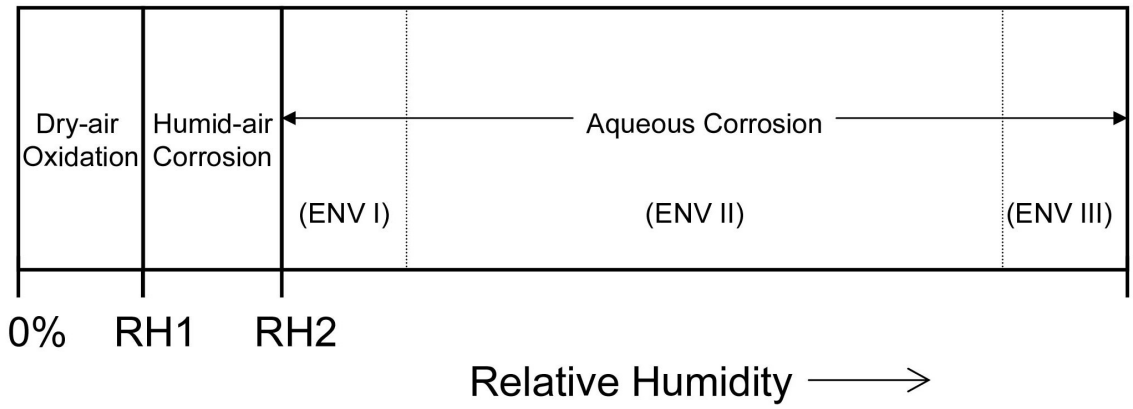

Figure 1. Schematic Diagram of the Evolution of the Corrosion Environment in the Potential Yucca Mountain Repository. The Relative Humidity of the In-drift Environment Determines the Initiation Time for a Specific Corrosion Mode. RH1 Denotes the Critical Relative Humidity for Humid-Air Corrosion, and RH2 Denotes the Critical Relative Humidity for Aqueous Corrosion .

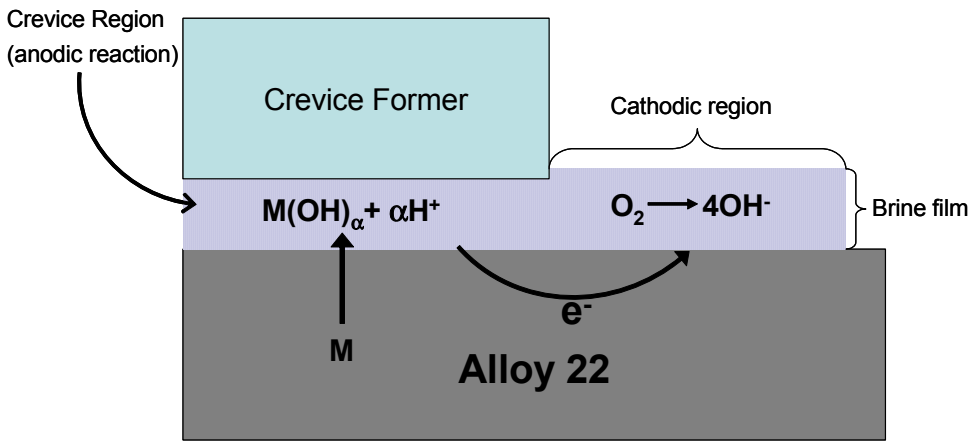

Figure 2. Schematic Diagram of the Crevice Corrosion Process. The Anodic Reactions Predominantly Occur in the Crevice Region, Whereas Cathodic Reactions Dominate in the Cathodic Region Located Adjacent to the Crevice.

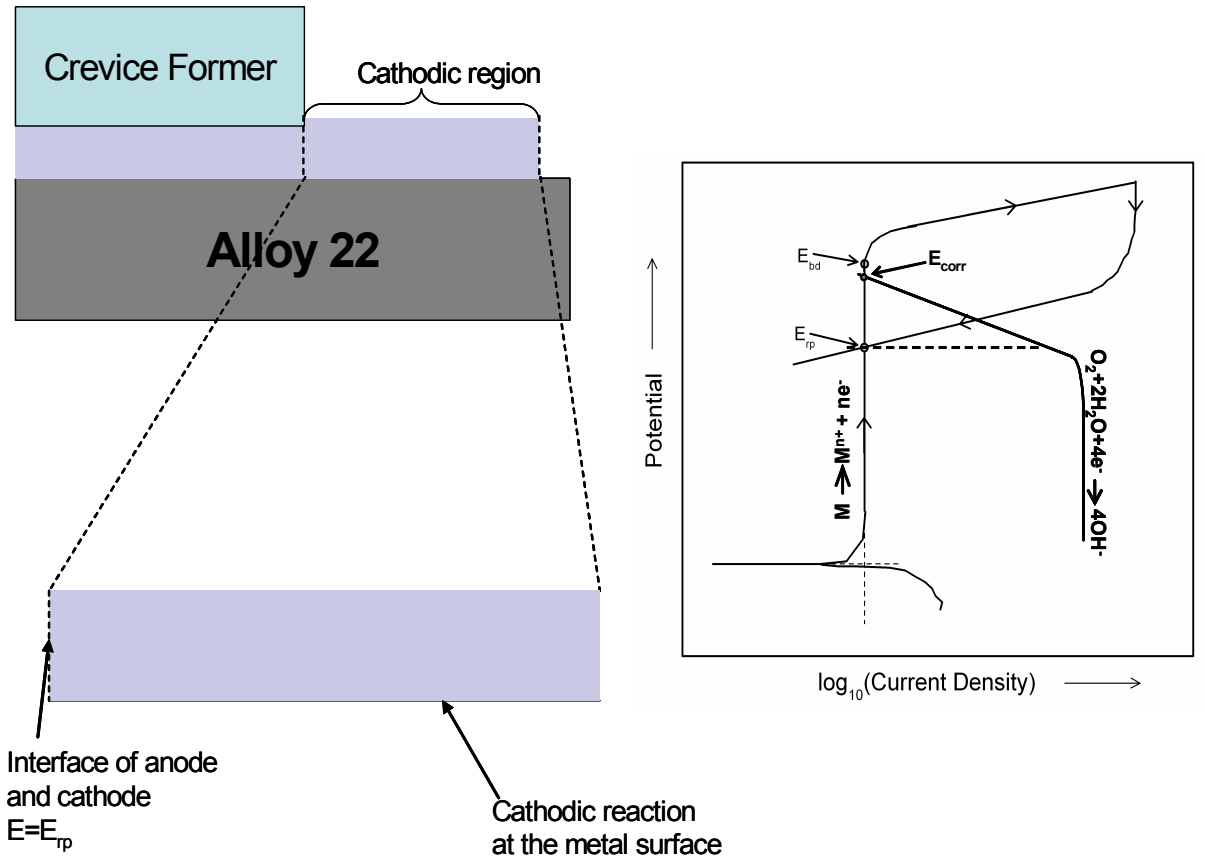

Figure 3. Schematic Representation of the Cathodic Region With Corresponding Cathodic and Anodic Polarization Curves. At the Interface of the Crevice and Cathode, the Potential Is Equal to the Repassivation Potential. The Excess Cathodic Capacity Is Generated in the Cathodic Polarization Curve When the Cathodic Region Electrode Potential Lies Between the Repassivation and Corrosion Potential.

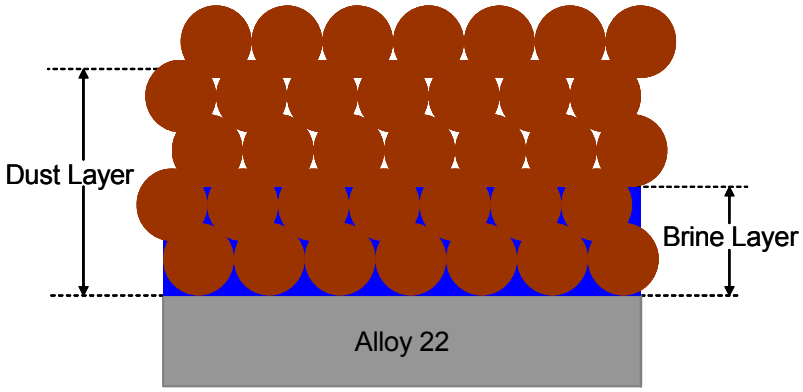

Figure 4. Schematic Representation of Dust Deliquescence Brine Layer and Dust Layer on Alloy 22 Surface.

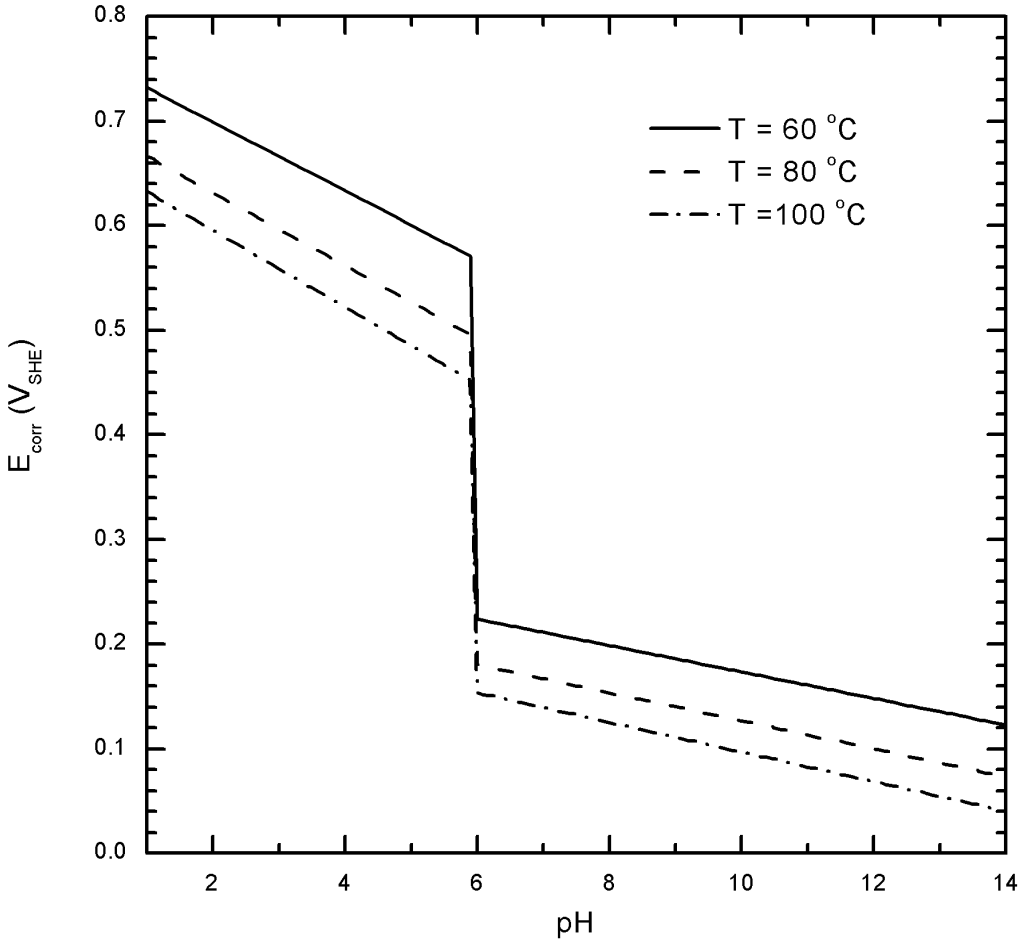

Figure 5. Corrosion Potential E_{corr} as a Function of pH at 60, 80, and 100 °C [140, 176, and 212 °F].

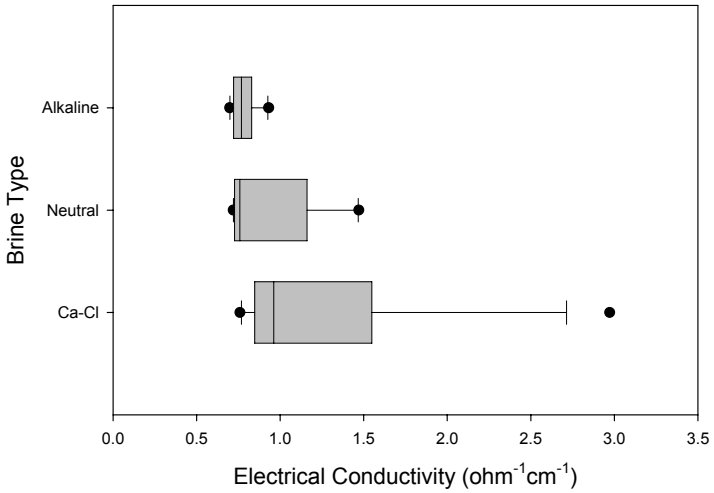

(a)

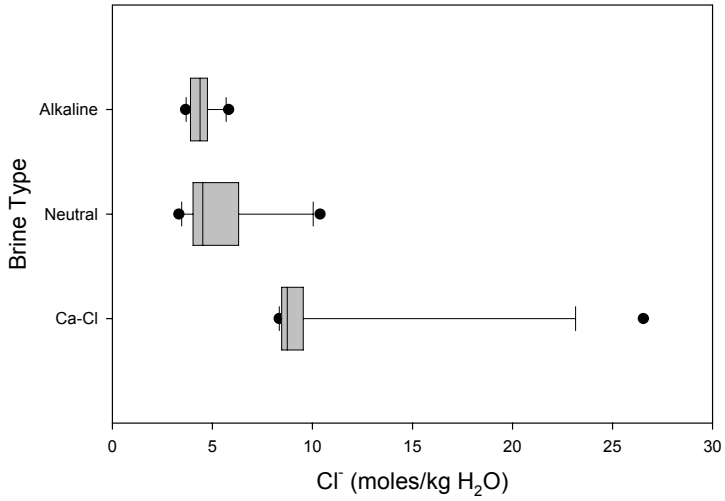

(b)

Figure 6. (a) Ionic Conductivity and (b) Chloride Concentration of Yucca Mountain Seepage Water Brines at 110 °C [230 °F].

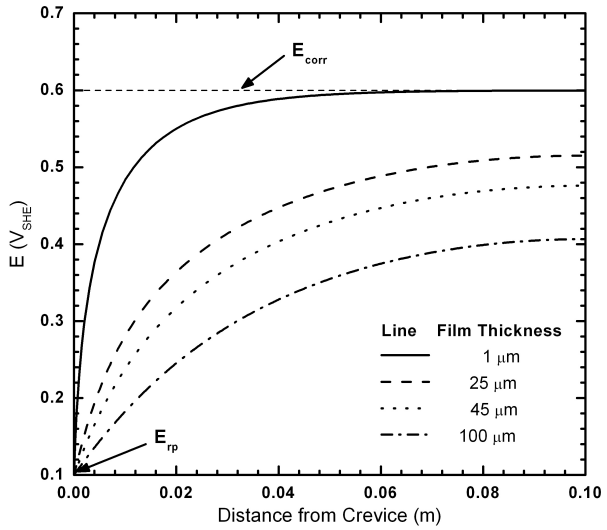

(a)

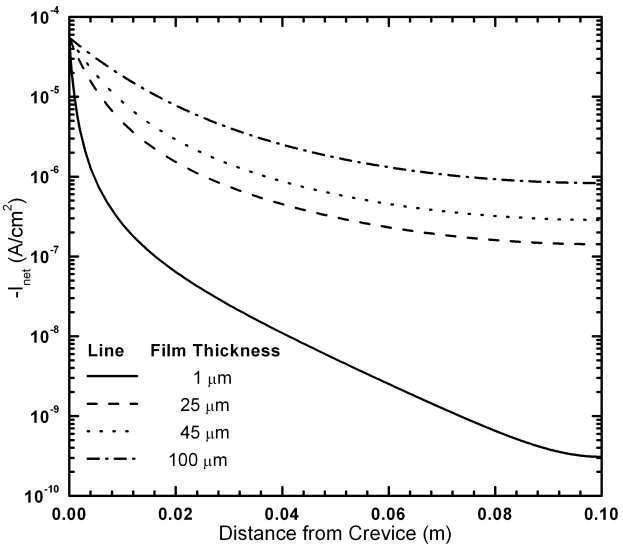

(b)

Figure 7. Electrode Potential and Current Density Distribution of Alloy 22 in the Cathodic Region. These Distributions Are Represented as a Function of Distance From the Crevice Region. The Electrolyte Brine Film Is Assumed To Be 0.1 m [3.94 in] Long and the Repassivation Potential Is Fixed at 0.1 V_{SHE}.

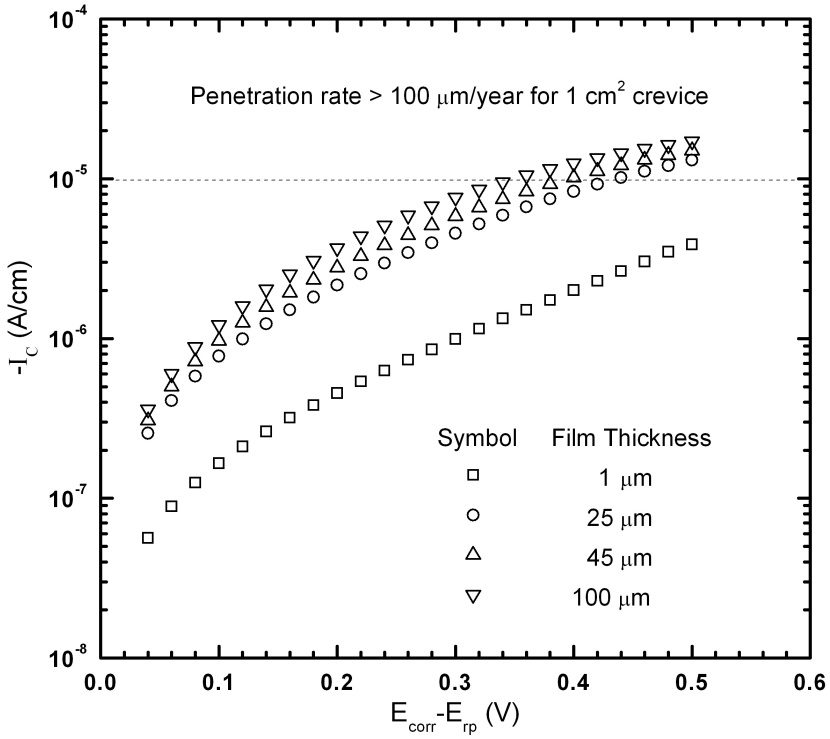

Figure 8. Cathodic Capacity of Alloy 22 in Dust Deliquescence Brine as a Function of the Difference Between the Corrosion Potential and the Repassivation Potential ($E_{corr}-E_{rp}$) for Various Film Thicknesses. The Corrosion Potential and Brine Film Length Are Fixed at 0.6 V_{SHE} and 0.1 m [3.94 in], Respectively. A Penetration Rate of 100 μm/yr [3.94 mils/yr] or Higher Is Expected for 1 cm^2 [0.16 in^2] of Active Crevice Region When the Cathodic Capacity Is Above the Horizontal Dash Line.

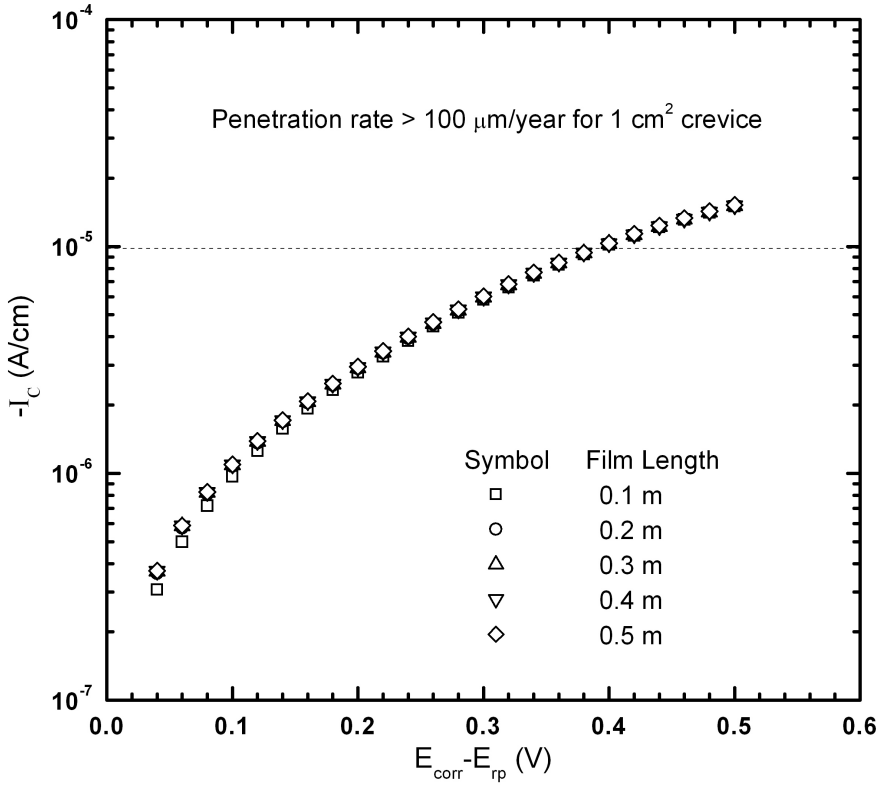

Figure 9. Cathodic Capacity of Alloy 22 in Dust Deliquescence Brines as a Function of the Difference Between the Corrosion Potential and the Repassivation Potential (E_{corr}–E_{rp}) for Various Brine Film Lengths. The Corrosion Potential and Brine Film Thickness Are Set Equal to 0.6 V_{SHE} and 45 μm [1.8 mils], Respectively. A Penetration Rate of 100 μm/yr [3.94 mils/yr] or Higher Is Expected for 1 cm^2 [0.16 in^2] of Active Crevice Region When the Cathodic Capacity Is Above the Horizontal Dash Line.

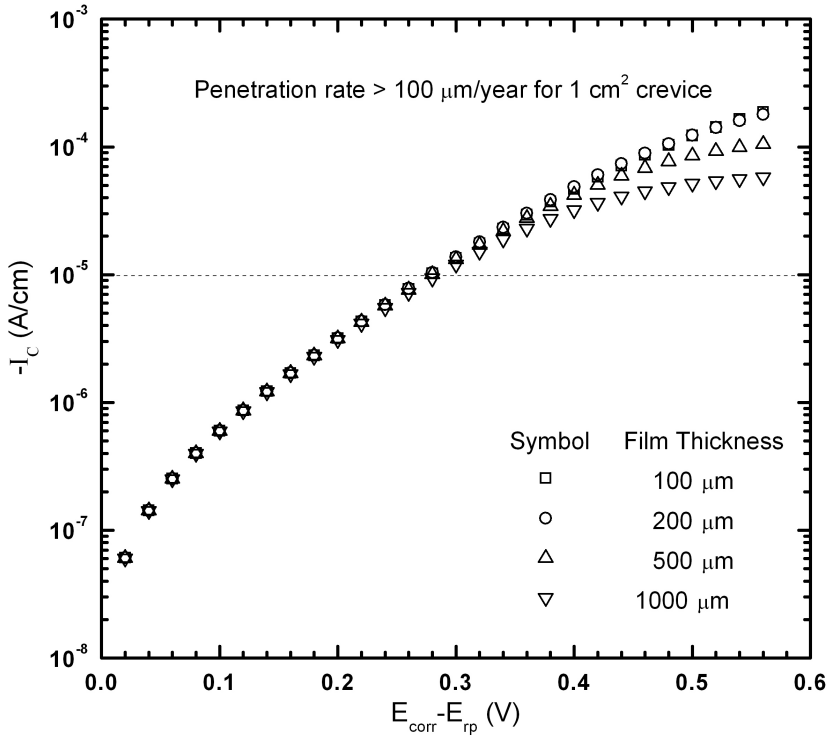

Figure 10. Cathodic Capacity of Alloy 22 in Seepage Brines as a Function of the Difference Between the Corrosion Potential and the Repassivation Potential ($E_{corr}-E_{rp}$) for Various Film Thicknesses At Brine Film Length Equal to 0.1 m [3.94 in]. A Penetration Rate of 100 μm/yr [3.94 mils/yr] or Higher Is Expected for 1 cm^2 [0.16 in^2] of Active Crevice Region When the Cathodic Capacity Is Above the Horizontal Dash Line.

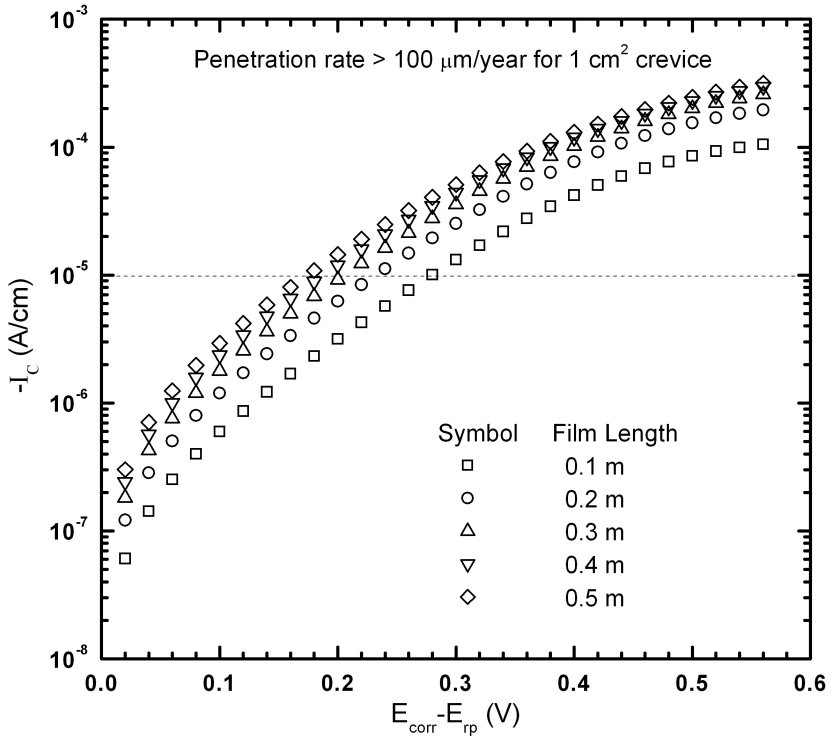

Figure 11. Cathodic Capacity of Alloy 22 in Seepage Brines as a Function of the Difference Between the Corrosion Potential and the Repassivation Potential (E_{corr}–E_{rp}) for Various Brine Film Length At Brine Film Thickness Equal to 500 μm [19.7 mils]. A Penetration Rate of 100 μm/yr [3.94 mils/yr] or Higher Is Expected for 1 cm^2 [0.16 in^2] of Active Crevice Region When the Cathodic Capacity Is Above the Horizontal Dash Line.